HHS Public Access

Author manuscript

J Chem Theory Comput. Author manuscript; available in PMC 2018 October 17.

Published in final edited form as:

J Chem Theory Comput. 2018 August 14; 14(8): 4487–4497. doi:10.1021/acs.jctc.8b00377.

Building Blocks of the Outer Membrane: Calculating a general elastic energy model for β-barrel membrane proteins

Henry J. Lessen, **Patrick J. Fleming**, **Karen G. Fleming**, and **Alexander J. Sodt***

T. C. Jenkins Department of Biophysics, Johns Hopkins University, *Eunice Kennedy Shriver* National Institute of Child Health and Human Development, National Institutes of Health

Abstract

The outer membranes of Gram negative bacteria are the first points of contact these organisms make with their environment. Understanding how composition determines the mechanical properties of this essential barrier is of paramount importance. Therefore, we developed a new computational method to measure the elasticity of transmembrane proteins found in the outer membrane. Using all-atom molecular dynamics simulations of these proteins, we apply a set of external forces to mechanically stress the transmembrane β-barrels. Our results from four representative β-barrels show that outer membrane proteins display elastic properties that are approximately 70 to 190 times stiffer than neat lipid membranes. These findings suggest that outer membrane β-barrels are a significant source of mechanical stability in bacteria. Our all-atom approach further reveals that resistance to radial stress is encoded by a general mechanism that includes stretching of backbone hydrogen bonds and tilting of β-strands with respect to the bilayer normal. This computational framework facilitates an increased theoretical understanding of how varying lipid and protein amounts affect the mechanical properties of the bacterial outer membrane.

Keywords

Continuum elasticity; Membrane proteins; Biomaterials; Gram negative bacteria; Outer membrane

Introduction

Mechanical forces are important to bacterial physiology and are suspected to play a significant role in pathogenesis.[1] Bacteria are subject to a myriad of forces covering a range of magnitudes within their native environments.[2] At the largest scale, bacterial colonies, microbial biofilms, and other multicellular assemblies found at solid-liquid interfaces experience shear force that primarily arises from the flow of the surrounding liquid.[3–4]

***Corresponding Author** alexander.sodt@nih.gov.

Author Contributions

The manuscript was written through contributions of all authors. All authors designed the simulation method and analysis framework. HJL analyzed the data. All authors have given approval to the final version of the manuscript.

ASSOCIATED CONTENT

Supporting Information. The following files are available free of charge.

File containing additional controls, analysis, methods, and figures for the above analysis. (Word Document)

These mechanical stresses affect the shapes and growth of the colonies,[5–6] the content of the extracellular matrix created by the bacteria,[2] and they can be utilized to further colonize the host surface.[7] Extracellular forces manifest their effects by altering gene expression and protein production in individual cells.[8] Previous research has primarily focused on mechanisms used by an individual bacterium to combat environmental stresses of this type. Typically, these experiments highlight the role of large macromolecular assemblies of proteins, such as pili, in anchoring the microorganism to a surface, to another bacterium, or to a host cell during pathogenesis.[9–10] It is becoming clear, however, that the response of the cell to external forces depends on more than just these tethering apparatuses. Almost all of the known cellular adhesion mechanisms are known to be either transmembrane or anchored to the membrane by some fashion,[9] and recent studies of *E coli* have shown that biological membrane content drastically affects their ability to adhere to surfaces and form biofilms.[7] These findings highlight the importance of understanding how different membrane components and compositions enable cellular responses towards mechanical forces.

Gram-negative bacteria present an interesting system to study the effect of membrane composition, because the cell envelopes of these bacteria are comprised of two membranes separated by an aqueous (periplasmic) space. The inner membrane (IM) is a phospholipid bilayer, with a molecular composition similar to standard biological membranes, whereas the outer membrane (OM) has a more uncommon composition and structure.[11] The most striking difference is the asymmetry of the OM. The inner leaflet is a phospholipid monolayer that is similar in composition to the IM, whereas the outer leaflet is thought to be mostly devoid of phospholipids.[11] Instead, the outer most barrier of *E. coli* is comprised of lipopolysaccharide, a large molecule consisting of three major components: Lipid A, the core oligosaccharide, and the O-antigen.[12] LPS has been shown previously to exhibit unique properties as both a permeability barrier and a virulence factor.[13] In addition to the distinct lipid content, the architectures of the integral membrane proteins found in the IM and OM are different. The IM is home to the more prevalent α-helical membrane proteins. In contrast, the OM is host to transmembrane proteins with a β-barrel architecture, termed outer membrane proteins (OMPs). Finally, there is a difference in the relative amounts of each macromolecules present in the IM and OM.

The molecular contrasts between the IM and OM suggest that these two biological membranes could have physiological distinctions in mechanical properties. Consider simply the weight ratios of their molecular components. The weight ratio of lipid molecules relative to protein in *E. coli* inner membranes is approximately 0.33/1.[14] This ratio can be loosely interpreted as having about 32 phospholipids per transmembrane protein if several assumptions about the average size of a phospholipid and IM protein can be made (see Supplemental Information). In contrast, the OM of *E. coli* has much lower lipid fractions with a dry weight ratio of lipid/protein equal to 0.14/1.[15] This ratio can be interpreted to mean approximately 4 phospholipids and 2 LPS molecules per OMP, which is significantly fewer lipids per protein than the IM (see Supplemental Information). These estimates are recapitulated experimentally by atomic force microscopy (AFM) studies revealing OMPs comprise between 60 to 75% of the surface area of the inner leaflet of E. coli OMs, which is estimated by the authors to be little more than ~3 LPS molecules and ~10 phospholipids per OMP.[15]

The distinct compositions of the IM and OM necessitate revisiting the conceptual understanding of the two membranes. The IM has long been represented by the fluid mosaic model (FMM)[16] in which cell membranes are generalized as large expanses of lipid bilayers with transmembrane proteins studded throughout. For this reason, the FMM is well described by the continuous elastic models of membranes that are based on the mechanical description of lipid bilayers alone. However, this mechanical model is unlikely to be an appropriate depiction of the OM due to the different protein to lipid ratio of the OM. Adding to the uncertainty of appropriating the FMM for the OM is the fact that OMPs have a different architecture as compared to the α-helical proteins found in the IM, and their elastic properties may be accordingly distinct. We begin to address this outstanding question in this study by developing and testing a molecular simulation method for interrogating the elastic properties of OMPs.

In recent years, computational studies have been demonstrated to accurately characterize the elastic properties of membranes[17] and proteins.[18–22] An additional utility of these simulations is the ability to resolve and monitor the many molecular degrees of freedom inherent to molecular dynamics (MD) simulations. This ability allows for the qualitative identification of molecular features that give rise to bulk properties, and thus it guides hypotheses on the basis of similarity. Therefore, all-atom MD simulations were chosen to apply elastic theory to elucidate mechanical properties of OMPs.

The framework described below computes an energetic constant (k_E, see Eq. 2) that models the elastic fluctuations of the radius of the OMP. This change in radius is resisted by the bonds and other interactions that are in the plane of the β-sheet. Due to the proportionality of the radius and circumference of a cylinder, radial strains and circumferential strains are equivalent, and thus the radial stress tests these molecular forces (the equivalence of radius and circumferential strain is tested explicitly in the Supplemental Information, Figure S14). The model provides the change in radius (strain) of the protein with applied force (stress). Following the presentation of the energetic constant and mechanism for β-barrel deformation is a discussion of how to apply the results of our study to answer specific questions of broad biological interest, such as “How does the area compressibility of a bilayer patch change with protein density?” or “How does the structure of a protein in a patch of membrane respond to external tension?” We conclude by revisiting the conceptual models used for OM studies.

Materials and Methods

Molecular dynamics (MD) simulations

We developed our energetic model using four OMPs from multiple bacteria. Three of the proteins studied were from *E. coli*: OmpW (an 8 stranded β-barrel), OmpA (8 strands), and OmpLA (12 strands). An additional protein (OpcA, 10 strands) from the organism *N. meningitidis* was also included to test the generality of the elastic model. The simulation systems were built using CHARMM-GUI.[23–24] The base structures used for building these systems were 2MHL (OmpW),[25] 1QJP (OmpA),[26] 1K24 (OpcA),[27] and 1QD5 (OmpLA).[28]

A symmetric phospholipid bilayer comprised of 1,2-dimyristoyl-sn-glycero-3-phosphocholine (DMPC) was used in our simulations for multiple reasons. Primarily, we chose the homogeneous DMPC bilayer because we wished to study the elastic properties of the proteins rather than the entire biological membrane. In this case, DMPC is a convenient biophysical tool that is easy to manipulate both experimentally and using simulations. Moreover, DMPC has a hydrophobic thickness well matched to that of the asymmetric OM.[29–30] Understanding the mechanical properties of various proteins in a homogeneous bilayer allows us to avoid potentially confounding effects of using asymmetric membranes that are comprised of multiple lipid types. This study thus establishes the tool using a system best able to be validated, yet with the flexibility to account for additional factors present in the biological system.

Each system was built in an orthorhombic cell and neutralized with 150 mM NaCl. Specific details regarding the number of ions in each of the systems is included in the Supplemental Information. The systems were equilibrated using the protocol set up by CHARMM-GUI.[24] Production runs of 300 ns were obtained using multiple supercomputing resources. The NAMD MD software was used to run the simulations with the CHARMM 36 force field under NPT conditions (313.15 K for OmpW and OmpLA/310.15 K for OmpA and OpcA and 1 atmosphere for all simulations).[31–32] The temperature was controlled using the Nose-Hoover thermostat, and the pressure was controlled with the Langevin piston. Newton's equations of motion were integrated using 2 femtosecond time steps. The damping coefficient for the constant temperature simulations was 1.0 $psec^{-1}$ and the bath was not coupled to the hydrogen atoms. The period for the constant pressure piston was 50 fsec and the decay time for the piston was 25 fsec. Long range electrostatics were calculated using the Particle Mesh Ewald[33] summation with a cutoff for short range electrostatics and Lennard-Jones interactions at 12 Å with a smooth switching function applied at 10 Å. Non-bonded pair lists were determined by a distance cutoff of 16 Å and were updated every 10 steps. Long range electrostatics and non-bonded interactions were evaluated at every step.

Three sets of starting coordinates to be used for the elasticity analysis were taken from the 300 ns of unconstrained simulation for each protein. The time points chosen for starting coordinates were taken at 100, 200 and 300 ns of the unrestrained production runs. Using these starting coordinates, short MD simulations (50 ns) were started and, during the simulations, a series of external uniform radial expansive forces was applied to the transmembrane C_α atoms of the β-barrel using the TclForces package for NAMD. The radial expansive force was applied to transmembrane atoms identified on the structure of the respective OMPs aligned using the Orientation of Proteins in Membranes (OPM) server[34–35] (see Supplemental Information). The applied force vector for an individual C_α was calculated in the following manner: 1) a vector was defined between the geometric center of the transmembrane C_α atoms and the individual C_α atom; 2) the Z component of the vector was subtracted; 3) the vector was normalized and its origin was set to the C_α coordinates; and 4) the vector was scaled to a specific force value. Figure 1 presents a representative example of the application of force vectors to the OmpW structure. Depiction of the force vectors on the other proteins can be found in the Supplemental Information. The total (scalar) radial expansive force was equal to the sum of all force magnitudes. The direction of each force vector was updated at each step during the simulation to ensure that the force was

always applied in the membrane (*XY*) plane. For each of the proteins, 6 separate forces were applied in triplicate, resulting in an additional 18 simulations per protein. The magnitude of the external forces applied to each protein can be found in the Supplemental Information. Only the last 30 ns of each 50 ns simulations with applied radial expansive force were used for post simulation analysis.

Elastic model of a generalized OMP

The energetic model was based on measuring geometric changes of the protein in response to applied forces. To calculate the elastic energy of deformation in response to applied stress, only the transmembrane β-barrel region of the OMP was used. The membrane is the primary medium of force application to OMPs, and we sought to mimic these forces in highly controlled fashion. In this work we compute strains displayed by the barrel as a result of the stress. This includes the radial (*R)* strain, the height (*h*) strain, circumferential strains, hydrogen bond (HB) strains, and strand tilt strains. With the exception of the radius and strand tilt, these strains are all computed by calculating changes in the distance between beta sheet backbone atom pairs (see “Computing pair strains” below). The resulting strains were used to calculate the elastic properties of the OMP. For the radius, the average distance of the protein backbone to the central axis of the OMP is defined as *R*, and the procedure for this calculation is detailed below. The average values for *R* in the absence of applied force is R_0. Deviations from the average will result in a unitless parameter, the strain (λ), defined as:

$$\lambda_{\text{radial}} = \frac{R - R_0}{R_0} \quad (1)$$

Equivalent strains can be computed for other metrics, such as strand tilt and height.

For parameterizing the elastic energy model, the radial strain results from the application of radial expansive forces. Height strains indicate the Poisson’s ratio, that is, the response of the material perpendicular to the applied stress.

At low levels of applied force, the stress-strain response is linear for an elastic model. Using this assumption, we employed a harmonic potential to define the elastic energy of barrel deformation (Eq 2).

$$U(R) = \frac{1}{2} k_E \lambda^2 = \frac{1}{2} k_E \left(\frac{R - R_0}{R_0} \right)^2 \quad (2)$$

In this equation, k_{E} is an energy constant with units of kcal mol^{-1}. This constant is unique to each OMP and describes the energetic penalty that results from net barrel strain. This potential was used to define an elastic force (F_{elastic}) responsible for restoring the value of *R* to R_0 by taking the derivative of the potential energy with respect to *R*.

$$F_{\text{elastic}} = \frac{dU(R)}{dR} = \frac{k_E}{R_0}\lambda = \frac{k_E}{R_0}\left(\frac{R - R_0}{R_0}\right) \quad (3)$$

At low magnitudes of uniform radial expansive force (F_{expand}), the sum of the barrel forces (F_{total}) can be set to 0 after the system has equilibrated under the applied F_{expand}. At equilibrium these forces must cancel and thus:

$$F_{\text{total}} = F_{\text{expand}} - F_{\text{elastic}} = 0 \quad (4)$$

With this relationship defined, substitution of F_{elastic} with equation (3) and rearrangement of variables results in the definition of k_{E} as:

$$k_E = \frac{F_{\text{expand}} R_0}{\lambda} \quad (5)$$

in units of energy (kcal mol^{-1}). This relationship provides a straightforward approach to calculating the value of k_{E} from simulation because F_{expand} can be applied precisely, and the values of R_0 and λ can be calculated directly from simulation. As long as the stress-strain response is linear, this method may be used to calculate the value of k_{E}.

Molecular forces maintain the shape and structure of an OMP. For example: hydrogen bonding, electronic structure leading to preferred backbone dihedral angles, and hydrophobic matching with the surrounding bilayer are all foundational energetic determinants of native structures. Deviations of the barrel size from the native state will naturally involve deformations of these features with the softest degrees of freedom contributing the most to the energetics. We hypothesized that backbone hydrogen bonding is one such soft degree of freedom and asked what portion of the elasticity these encode. The contribution of hydrogen bonding to k_E can be estimated by mapping the proportionality of hydrogen bonding to radial OMP strains in conjunction with an effective hydrogen bonding force constant. This phenomenological term ($k_{\text{E,HB}}$) was calculated by measuring the distribution of fluctuating HB strains around their average value ($R_{0,\text{HB}}$). The variance of these fluctuations was used to calculate $k_{\text{E,HB}}$ according to equation (6):

$$k_{E,HB} = \frac{k_{\text{B}} T}{\sigma_{HB}^2} \quad (6)$$

where k_{B} is Boltzmann's constant, T is the absolute temperature, and σ_{HB}^2 is the variance of the HB fluctuations. The strain for HBs orthogonal to the membrane normal will be akin to λ_{radial}, because the circumference and radius are proportional. The strain for HBs deviating from the XY plane will depend on Poisson's ratio, which gives the strain orthogonal to the

main stress. However, because the HBs are not perfectly orthogonal to the membrane normal they experience only the projection of the in-plane stress, which is computed by the cosine of the angle formed by the HB vector and a vector tangential to the protein surface in the XY plane (see Supplemental Information). The squared cosine of this angle was thus used to project the effect of $k_{E,HB}$ calculated from Eq 6 into the tangential deformation and similarly to account for the forces experienced by the HBs during radial expansion (corrections detailed in the Supplemental Information). With these corrections, the sum of the HB energy constants was compared to the elastic constant of the barrel.

Additional Structural Assumptions used in Elasticity Calculations

In the developed OMP elasticity model, k_E relies on the validity of the calculated radius R (i.e. is this a reliable measure of the structural properties of the OMP). In the Supplemental Information, we demonstrate that the calculation of R is both robust for each individual protein and that the omission of a random subset of residues does not drastically change the value of R. This result demonstrates that small changes of R in response to expansive force are both significant and reports a real measurable strain on the transmembrane structure. The equivalence of independently calculated radial and circumferential strains (Figure S14 of Supplemental Information) provides additional validation of R.

Additional structural assumptions allow for the determination of fundamental *material* elastic constants. The Young's modulus (E) is a property of isotropic materials that relates the axial strain to an axial stress, with the perpendicular directions "free".[36] We note that although the OMP is clearly not an isotropic material, the same molecular forces are at play in a larger scale assembly of beta sheets, like spider silk. Building a *per-unit volume* material model of an OMP, e.g., the Young's modulus, then allows for a comparison between the stiffness of materials with vastly different length scales. To report the direction to which the Young's modulus applies, we first defined the orientation of the strands relative to the applied force. Qualitatively, the strands are oriented approximately along the bilayer normal. Under this assumption, the stressed and measured strain direction is the circumference of the OMP of resting length $2\pi R_0$, and thus the Young's modulus refers specifically to this direction. A second aspect to this definition is to clarify the amount of material that gives rise to the elastic properties of the OMP. More simply we ask, "what is its thickness?" Given the same radial deformation (expanding the circumference of the cylinder) the assumption of a very thin shell would imply a much higher stiffness than for a thick shell, because much less material would be responsible for yielding the same strain. In terms of the Young's modulus, the strain energy is given by:

$$U = \frac{1}{2} V E \lambda^2 \quad (7)$$

where V is the resting volume of the material, λ is the material strain and is equal to λ_{radial} because the lengths of interest are proportional to R. By combining equations 2 and 7, the Young's modulus was computed as:

$$E = \frac{k_E}{V} \quad (8)$$

A second useful parameter that was learned from the simulation data was the Poisson's ratio (ν) of the protein related to the change in the height of the protein orthogonal to the applied stress. This parameter reports on the ratio of strain in orthogonal directions and was defined as follows:

$$\nu = -\frac{\lambda_{\text{height}}}{\lambda_{\text{radial}}} \quad (9)$$

where the designation of both height and radial strain (Eq 1) was used here to denote deformations in either the height or the radius of the transmembrane barrel.

Analysis of k_E from MD Simulations

The method for calculating the radius of the protein (R) was key to determining the value of k_E for OMPs. To perform this calculation, the protein first was aligned to a reference set of coordinates to remove the effects of changes in tilt angle of the central axis of the OMP. Then, a vector from the geometric center of the transmembrane C_α atoms to a specific C_α atom was calculated. The z component was subtracted from this vector, and the magnitude of the remaining vector was taken as the cylindrical radius for this specific atom. This procedure was carried out for each transmembrane C_α in 20 ps time steps of the 30 ns analysis region of the trajectory and was used to obtain the time average for the radial distance of each transmembrane C_α atom. The mean of the time averaged radial distances for the individual transmembrane C_α atoms was used to calculate the radius of the OMP β-barrel. The average value for the distance, R_0, was calculated from the last 250 ns of the 300 ns unrestrained MD simulation, the λ is calculated using Eq 1. Finally, to account for differences in OMP orientation in the bilayer (i.e. differences in tilt angle), the force was scaled by the cosine of the tilt angle. This orients the force so that it is always normal to the plane tangent to the protein surface. The differences in tilt angle are negligible compared to statistical error but were included for completeness. The value of k_E was calculated by multiplying the slope of the strain *versus* stress relationship by R_0 (Eq 5). All linear regression analysis was performed using the analysis program, *R*.

A critical question for this analysis is "What constitutes an elastic deformation from the resting state?" β-barrel proteins are extremely stable in the membrane,[37–39] and the target structural variability investigated in this work includes only fast relaxing fluctuations critical to the barrel structure. This principally includes fluctuations of the transmembrane β-sheet strands. To ensure that only small, fast relaxing perturbations were resulting from our applied forces, we collected the individual strains for each atom from all the simulations where the expansive radial force was applied. These distributions were plotted and examined for abnormalities (see Supplemental Information). The ideal distribution of individual strains was a narrow normal distribution centered around the total barrel strain for that force. This

indicated that the stress was uniformly felt by all parts of the transmembrane barrel, and the elastic criterion was met.

Runs that exhibited broad, tailed strain distributions indicated the presence of excessive outliers. If excessive outliers were present, the elastic criterion was violated due to the applied expansive force, and the run was discarded. Including these outliers would have broken the intended elastic assumption and presumably lead to much lower apparent elastic moduli. The cause of these outliers was presumed to be large deformations to the native structure of the OMP. Structural variations, such as partial unfolding, violate the elastic assumption in part because they would likely relax slowly. In view of the long-term goal for this study – to include OMP elasticity as an element in larger models of biological membranes – internal degrees of freedom would appear inelastic if they relax more slowly than the changing structure of the larger membrane model in which they are included.

Elasticity analysis of OMPs

The value of k_E can be converted into the Young's modulus using Eq 8. This conversion requires knowledge of the volume of the cylindrical shell, which is the geometric model used to approximate the OMP. To determine this parameter, the structural elements that give rise to the elastic properties of the OMP must be defined. Motivated by the idea that the β-barrel conformation is maintained by backbone HBs, we hypothesized that the main load-bearing element of the transmembrane β-barrel is the protein backbone, and we used Voronoi analysis to calculate the volume of these backbone heavy atoms defining the cylindrical shell (see Supplemental Information). An estimate of the barrel volume was obtained by summing the volumes of the individual backbone heavy atoms. The Poisson's ratio was calculated using Equation (9), where the λ_{radial} is the strain of the barrel radius and λ_{height} is the strain of the cylindrical shell height computed using pairs of backbone atoms aligned along the barrel axis.

Analysis of $k_{E,HB}$ from MD Simulations

To calculate HB parameters between transmembrane backbone functional groups, the VMD "measure hbonds" method was used. These parameters are measured from the same simulations used to calculate k_E. In order to classify as a HB, the interaction had to be observed for 150 ns of the simulation. The average length of each HB in the resting state was calculated from the last 250 ns of unrestrained simulation. These average lengths were used as the $R_{0,\text{HB}}$ values and subsequently employed to calculate their normalized fluctuations. The distribution of these fluctuations allowed us to calculate $k_{E,HB}$ using Eq 6, where σ^2_{HB} was the variance of this distribution (see Supplemental Information). The $k_{E,\text{HB}}$ value was then corrected using the previously mentioned cosine term.

To examine if the average HB response to radial expansive force was also linear, the average λ_{HB} values for individual HBs at the different expansive forces were calculated. Only HBs that were present in more than 15 ns of the analyzed 30 ns simulations were used to calculate $k_{E,\text{HB}}$. Finally, the force per atom was modified using a cosine term to obtain the force component in line with the vector of the HB defined using the heavy atoms. For details regarding the calculation and application of the angular term, refer to the Supplemental

Information. A weighted linear regression analysis was used to calculate the stress/strain relationship for the HBs. Observed HB strains reflect, in part, the softness of this degree of freedom relative to others that maintain the barrel structure, for example, covalent bonds. As a simple check, the strains of covalently bonded atoms (e.g. the backbone carboxyl double bond) were computed with the same tools and the strains were found to be over 50 times smaller than those for HBs. The values of $k_{E,HB}$ calculated from both the HB fluctuations and the stress vs strain relationship were compared to one another as an independent control (see Supplemental Information).

Computing pair strains

In addition to the radius and HB lengths, strains can also be measured for the distance separation between any pairs of atoms. The distances between atom pairs with nearly identical x and y coordinates, but which are separated in z, are the basis for *height* strain measures. A pair at the same value of z but whose separation defines a vector nearly tangent to the cylindrical surface is the basis for a *circumferential* strain measure, expected by the cylindrical assumption to be equivalent to the radial strain. For each backbone atom in the strand region of the OMP (with barrel axis aligned on z), height and circumferential strain pairs were computed by selecting the atom on the next strand that is most aligned with or perpendicular to the z axis, respectively. The beginning and ending of the strands for each protein are generally at the top and bottom of the barrel; and these residue identities are reported in the Supplemental Information. The average pair length was computed using the unbiased reference simulation to define the equilibrium length. Fractional strains were then computed and averaged for each pair in each simulation as a function of force applied. The same procedure was used to compute HB strains between donor/acceptor pairs, as well as for backbone covalent bonds as a simple control.

Results

OMPs demonstrate an elastic response to wide range of mechanical forces

Almost all simulations subjected to radial expansive force obeyed the elastic criterion detailed above. From these simulations, the average radial strain was calculated for the barrel at each expansive force and the series was fit using a weighted linear model (Figure 2). The assumption of linearity holds over the range of forces used for all proteins investigated, despite evidence for the need of non-linear elasticity for function in some soluble proteins.[18, 40] Furthermore, the fact that this linear trend is observed in all proteins measured, despite the differences in size, function, and species origin, is suggestive that this elastic behavior is a general property of transmembrane proteins with a β-barrel architecture.

Interestingly, the OMPs in this study demonstrate a large range of k_E values. The energy constants obtained from our analysis range from 12,800 to 35,000 kcal mol^{-1} and are summarized in Figure 3. Qualitatively, a comparison of k_E shows that OMP mechanical properties depend on more than just strand number. Both OmpA and OmpW are 8 stranded β-barrels, but their k_E values are separated by more than a factor of two (twice the energy for the same deformation). However, k_E is difficult to relate to other biological materials because there is no experimental equivalent. In order to put OMPs in the context of other

cell envelope components, we must convert these number to other, more universal constants. We did this by reducing the complexity of OMP structure using a simplified geometric assumption. We then further utilized the model to describe the OMP as an elastic material, which can be readily compared to other cell envelope components.

The material volume of an OMP is approximated by a hollow cylindrical shell

We chose to model the OMP as a hollow, cylindrical shell because this was most representative of general OMP architecture (Figure 4). Our assumption regarding the nature of the "elastic material" of an OMP was that backbone interactions, primarily secondary structure, are the primary determinant of OMP elasticity (we will test this assumption later). The volume of all transmembrane backbone atoms was measured for the each β-barrel (method described in the Supplemental Information). The calculated "shell thickness" values ranged from 4.1 to 4.2 Å (see Supplemental Information). Although this number is larger than the diameter of a carbon atom (~1.4 Å), its value is not surprising in view of backbone thermal fluctuations, atomic packing, and presence of hydrogen atoms omitted from the volume analysis. This volume reflects the amount of space consumed by the OMP backbone considering both the membrane and other protein atoms. The energetics of the "material" represented by volume depends on the continuous, β-sheet structure signature to OMPs. Properties, such as surface area, can also be approximated using this geometric model.

OMPs are much more rigid than lipid bilayers and other structural elements in cells

Elastic material constants provide a common language for comparing membrane components. Their utility originates from two main points: 1) material properties can be experimentally verified and 2) MD simulations have been shown to reliably reproduce these experimental values.[18] By converting our theoretical value of k_E to a material property, we extend the ability of our theory to generate testable hypothesizes regarding the effect of OMPs on general bilayer properties. The Young's modulus (E), which reports on the linear elastic properties of a material in response to unidirectional force,[17] is commonly used to describe lipid bilayers. As stated in the Methods, E has a direct relationship to the strain energy (Equations 7 and 8) as long as the volume of the "material component" can be obtained. Using the volume calculated above, the Young's modulus was calculated using Equation 8. The values of E measured for all OMPs range from 20 to 45 GPa. In Figure 5, we compare the elasticity of OMPs to other biological materials.[18, 41–42] Simply put, OMPs are more rigid than many other structural components of the cell.

The Young's moduli of all OMPs in this study are approximately three orders of magnitude larger than the known values measured for phospholipid bilayers, ~20 MPa.[43] This result indicates that increased rigidity in the OM may derive from the high density of OM β-barrel proteins, in addition to the changes in the lipid composition. Our model of OMP elasticity also provides a value of Young's modulus larger than those measured for other structural elements found in biology, such as bacterial capsids (~2 GPa) and microtubules (~1 GPa).[21–22, 44] Finally, OMPs demonstrate similar elastic properties to materials proposed to derive their elasticity from β-sheet secondary structure, such as spider silk.[18] The similarities between the values of E for spider silk and OMPs provided a starting point for the second

half of our analysis. We now provide an investigation of the molecular mechanism behind OMP rigidity.

β-sheet secondary structure is a primary determinant of OMP elasticty

While useful in providing an avenue for comparison of between other biological materials, elastic constants such as E are bulk properties and do not inform on the molecular mechanism behind elasticity. To gain insight into the how/if β-sheet secondary structure acts as the driving force behind OMP elasticity, we analyzed the strain response of backbone HBs to expansive stress. A strain was expected to manifest on the backbone HBs while OMPs were subjected to force, because they are relatively weak interactions. This strain was observed and allowed us to calculate an average energy constant for hydrogen bonding ($k_{E,HB}$) (see Supplemental Information). After determining the $k_{E,HB}$ for each OMP, we assessed the relative contribution of backbone HBs to the total k_E of the OMP β-barrel. The spring model energy is additive, so we did this by multiplying $k_{E,HB}$ by the number of transmembrane HBs and dividing by k_E. This result is summarized in Figure 6 and shows that the contributions of backbone HBs constitute a significant percentage (~30%) of the greater elasticity constant, assuming the idealized OMP surface is covered by these bonds. Unexpectedly, the contribution of backbone HBs is approximately the same across all proteins. The fact that backbone HBs make an equal contribution to the elastic energy of this diverse set of proteins provides support to the idea that backbone hydrogen bonding ubiquitously influences the mechanical properties of OMPs. Furthermore, it provides direct evidence that β-strand dynamics are directly involved in the response of OMPs to mechanical stress.

OMPs reduce their barrel height as they are stressed in the plane of the membrane

Materials typically respond in the unstrained direction to accommodate stress.[45] For example, the molecular interactions of the sheets may favor constant area, in which case the height strain would be the negative of the lateral strain. The HB strains are smaller than the radial or circumferential strain, suggesting that there is more to barrel expansions than simply the stretching of HBs. An additional mechanism for accommodating expansive stress, suggested by the small HB strains, is changing the β-strand spacing through strand tilting with respect to the barrel axis. Using the method described above (in “Computing pair strains”**)**, we calculated the height strain of atom pairs to investigate whether changes in barrel height occurred in response to stress in the plane of the membrane. A linear decrease in height in response to increasing radial expansive force was observed for all OMPs. Using these height strains (λ_{height}), we calculated an effective Poisson’s ratio for each protein using Eq 9 (see Supplemental Information). The Poisson’s ratio values are summarized in Figure 7. All of these values are greater than 0, which qualitatively indicates that the OMP reduces its height in response to being stretched in the radial direction.

To understand the molecular origin of the Z strain, we also calculated the change in β-strand tilting. The end-to-end distance of the strand was defined as l. The height of the barrel will be equal to $l \cos \theta$, where θ is the angle between the strand and the barrel axis (see Supplemental Information for the calculation of the barrel axis). Assuming the strain in l is negligible, the height strain should be proportional to the “strain” in $\cos \theta$:

$$\lambda_{\text{height}} \approx \frac{\cos\vartheta - \cos\vartheta_0}{\cos\vartheta_0} \text{ (tilt mechanism)} \quad (10)$$

Comparisons between λ_{height} and the strains in cos ϑ indicate strong linear correlation, see the Supplemental Information. It is important to note that all OMPs, irrespective of size or function, show the same molecular response to external stress. Our analysis reveals a general mechanism for stress accommodation in β-barrel membrane proteins.

Discussion

The β-strands of stressed OMPs reorient by tilting which stretches HBs

An important outcome from this study is that OMPs have a shared molecular mechanism for responding to mechanical stress in the plane of the membrane. While the amount of force required to deform OMPs varies from protein to protein, the data demonstrate that two major types of structural changes result in elastic strain in the OMP. The first is that HBs are stretched in response to the radial stress. This mechanism is intuitive for two reasons: 1) hydrogen bonding is a “soft” interaction and thus will be more sensitive to small magnitude forces; and 2) the backbone HBs are in the plane of the barrel circumference, where the radial strain also manifests, and therefore should elongate to accommodate the enlargement of the protein. Essentially, we find that backbone HBs impose explicit distance restraints on the magnitude of the strain any given barrel can undergo without entering the inelastic regime of deformations. The second mechanistic deformation we observed for all OMPs studied is that the β-strands appear to slightly, but significantly, change their angle relative to the barrel axis in response to radial stress. This yields a wider and shorter barrel. The structural change manifests in the Poisson’s ratio. We speculate that the two phenomena are linked because it is reasonable to assume that the decrease in barrel height is modulated by how much the HBs can deviate from their preferred geometry.

While we determined how transmembrane β-structure determines OMP elasticity, we speculate there may be additional factors. It is unclear from our simulations the extent that sidechain interactions alter mechanical stability of OMPs. In addition, other sequence specific effects, such as β-strand propensity, could also impact the magnitude of k_E. More studies, with additional proteins, will be required to address the importance of these or any other interactions on OMP mechanical properties. We must also mention that continuous extensions of β-sheet structure from the transmembrane region to the extracellular loops could enhance the rigidity of OMPs. From our set, OpcA was the only protein that retained residual β-barrel structure in the extracellular region of the protein. With only one data point, we cannot definitively state that soluble extensions of the transmembrane barrel influence its elastic response. However, given the mechanism of strand tilt, the extended, soluble barrel structure of OpcA should deform in the same way and, thus, influence deformation energetics to the same extent as transmembrane strands. At this time, we speculate that extensions of the transmembrane barrel will serve to increase the elastic energy constant k_E. Future studies can be used to identify if the extension (or reduction) of β-sheet structure in OMPs plays a significant role in their mechanical properties.

OMPs meaningfully influence OM material properties

Having identified a generalized mechanism for β-barrel elastic deformations, we extend our focus to the role of OMPs in altering the material properties of the composite bilayer. From previous studies, it has become obvious that the fluid mosaic model should be altered when describing the OM given the relatively large fractional protein composition (60–75% by projected area).[15] Here, we consider a simple model of the OM lateral elastic membrane energy E_M with two components. First, a lipid component with area A_0^{L} has area compressibility modulus K_A^{L}. Second, N proteins with total cross-sectional area $N\pi R_0^2$. The model energy, including an external tension σ can be written as:

$$E_M = \frac{K_A^L}{2} A_0^L \lambda_{\mathrm{L}}^2 + \sum_{i=1}^{N} \frac{k_{E,i}}{2} \lambda_{\mathrm{radial},i}^2 - \sigma(\lambda_L A_0^L + \sum_{i=1}^{N} \lambda_{\mathrm{radial,i}} 2\pi R_{0,i}^2) \quad (11)$$

Here there are two independent strains, the lipid area strain λ_{L} and the OMP radial strain $\lambda_{\mathrm{radial}}$. The equilibrium strains are determined by minimizing the energy, or equivalently setting the derivatives of the energy with respect to the strain to zero. Solving for the equilibrium strains provides the equations:

$$\lambda_{\mathrm{L}}^{\mathrm{eq.}} = \frac{\sigma}{K_A^L} \quad (12)$$

$$\lambda_{\mathrm{radius,Total}}^{\mathrm{eq.}} = \frac{\sigma\, 2\pi R_{0,Total}^2}{k_{E,Total}} \quad (13)$$

where $R_{0,Total}^2 = \sum_{i=1}^{N} R_{0,i}^2$, $\lambda_{radius,Total}^{eq} = \sum_{i=1}^{N} \lambda_{radial,i}^{eq}$, and $k_{E,Total} = \sum_{i=1}^{N} k_{E,i}$ where i refers to the individual proteins. A quantity, which will be denoted $K_A^P = \frac{k_{E,Total}}{2\pi R_{0,Total}^2}$, is analogous to the area compressibility of the lipid patch. The value for the studied OMPs is computed to be between 19 and 50 N/m (Figure 8), about 70 to 190 times larger when compared to 0.265 N/m for a simple lipid like DOPC.[46] Consider that the compressibility modulus of the protein is a factor f_k higher than the lipids, $K_A^P = f_k K_A^P$, and that the protein area fraction is f_A higher: $N\pi R_0^2 = f_A A_L$. Interestingly, the value of f_A will depend on the individual identities and relative amounts of each OMP in the OM, it addition to the relative amounts of surface area to lipid. In this case, the effective area compressibility modulus of the mixture, K_A^{mix}, is:

$$K_A^{\text{mix}} = \frac{(1 + f_A) f_K K_A^{\text{L}}}{f_A + f_K} \quad (14)$$

With f_K being more than a factor between 70 and 190 higher than the lipid region, the effective area compressibility modulus of the mixture is scaled up by $(1 + f_A)$. With two to three times more protein than lipid, this increase is considerable. The picture becomes even more interesting when considering that K_A^{L} reflects *bulk* lipid, which is able to deform at nearly constant volume. That is, the thickness of lipid patches decreases as its area increases. However, when surrounded by stiff protein, the lipids will maintain hydrophobic matching, and now must effectively curve to increase or decrease in area. How the small patches of interstitial lipid between OM porins behave will be a critical factor in determining the overall elasticity, perhaps dramatically increasing the effective area compressibility modulus. In addition, the Poisson ratio for the protein will also play a role in describing how lipids maintain hydrophobic matching by describing the amount of thinning that proteins experience as a result of external tension.

Variation in OMP elastic properties can have biological implications

Our results also shed light on the biological impact of how changing the OM can affect the mechanobiology of the cell. For instance, OMPs have been shown to exist in confined diffusion areas referred to as “OMP islands”.[47] Due to the large size of these domains (~500 nM), we speculate that islands could be home to multiple OMPs, each with different mechanical properties. Furthermore, the spatial organization of OMPs is limited by their diffusion properties.[47] The result of these “poorly mixed” (ie non-random) OMP populations in the OM could definitely give rise to local domains in the OM that exhibit unique biomechanical properties. Could OMP islands play ancillary roles in supporting the function of large macromolecular machines required for adhesion or motility by fine tuning the local elastic properties of the membrane by using protein synthesis? This is a definite possibility, given the array of elasticity constants observed from our representative set.

Additionally, it is interesting to explore how bacteria control the global mechanical properties of their membranes through expression of different OMPs. Using *E. coli* as an example, OmpA has a high expression (~100,000 per cell), OmpW has intermediate expression (~4,000 to 40,000 per cell depending on the study), and OmpLA has relatively low expression (~400 per cell).[48–49] An interesting finding from looking at the *in vivo* copy number of each protein in our study is that the most rigid protein from *E coli* (in this study) is also one of the most prevalent of all OMPs. On one hand, this result could simply be serendipitous. However, the function of these proteins hints at a different story. Both OmpA and OpcA are involved in structural roles of the OM,[27, 50] whereas OmpLA is a phospholipase[28, 51] and OmpW (though its true function is unconfirmed) is implicated in transport.[52–54] The elevated expression of OMPs with more rigid elastic properties could reflect the greater role of the OM as serving as a mechanical barrier for the bacterium.[50] Understanding how a protein’s function is tied to its mechanical properties could provide insight into the coupling of protein synthesis and OM organization. More studies will allow

us to test this hypothesis. These are a few examples of how the biomechanics of OMPs can have a physiological impact on bacteria.

OMPs are the most rigid component of the Gram negative cell envelope

Finally, we will complete the discussion of β-barrel elasticity with a comparison between the material properties of OMP and other cell envelope materials. We reiterate that the mechanical properties of OMPs are suggested by this work to be orders of magnitude larger than any lipid bilayer in our knowledge. In addition, as the OM is more protein dense than the inner membrane, our composite model of the membrane suggests that then OM should be the more rigid of the two bilayers (see Supplemental Information). The cell envelope of Gram negative bacteria has one other structural component worth mentioning: peptidoglycan. Peptidoglycan is a mesh-like polymer and is widely thought to be the main source of cellular rigidity.[55–56] This knowledge comes from the observation that the inhibition of its biogenesis or degradation during bacterial growth results in lysis and subsequent cell death.[57] The experimentally determined Young's modulus for peptidoglycan appears to depend on its level of hydration. Dry peptidoglycan has been measured to have a Young's modulus of ~20 GPa, while fully hydrated peptidoglycan (as determined from stretching of a bacterial thread) has a significantly decreased Young's modulus valued around ~10 MPa.[58] In reality, the peptidoglycan is most likely partially hydrated, which tensile properties in between fully hydrated and dehydrated values.[59] Even when compared to peptidoglycan, our studies suggest that OMPs are the one of the most rigid materials in the Gram negative bacterial cell envelope. Further studies will be required in order to elucidate the complex role different components play in determining the elasticity of the cell.

In conclusion we will attempt to reconcile the results of our analysis with the current literature with regards to OM structure. Primarily, we would like to propose an update for the conceptual model of the biological OM. Combining our knowledge of OMP stiffness with the information from the AFM study and vastly different weight ratios,[15] we propose that the OM should be thought of as a wall composed of OMP bricks connected by lipid mortar. Our model has not only provided more insight into the nature of the foundational units of the OM, but gives a new avenue of inquiry with the goal of creating a more complete and thorough understanding of the bacterial OM. The ability of this model to provide a more accurate description of the mechanical properties of the OM serves as motivation for additional studies on OMPs of different sizes and functions in order to identify overarching trends of OMP elasticity.

Supplementary Material

Refer to Web version on PubMed Central for supplementary material.

ACKNOWLEDGMENT

AJS was funded by the intramural program of the *Eunice Kennedy Shriver* National Institute of Child Health and Human Development of the National Institutes of Health (NIH). The Biowulf high performance computing resource was used for a portion of the simulations. The other simulations were using computational resources from the Maryland Advanced Research Computing Center (MARCC) and XSEDE MCB120050.

Funding Sources

NIH Grant NIH Grants R01 GM079440 (KGF) and T32 GM008403

XSEDE Grant MCB120050

NIH Intramural Research Program

ABBREVIATIONS

IM	(bacterial) inner membrane
OM	(bacterial) outer membrane
OMP	outer membrane protein
OmpW	outer membrane protein W
AFM	atomic force microscopy
HB	hydrogen bond
OmpLA	Outer membrane phospholipase A
OmpA	Outer membrane protein A

REFERENCES

1. Auer GK; Weibel DB, Bacterial Cell Mechanics. Biochemistry 2017, 56 (29), 37103724.
2. Persat A; Nadell CD; Kim MK; Ingremeau F; Siryaporn A; Drescher K; Wingreen NS; Bassler BL; Gitai Z; Stone HA, The mechanical world of bacteria. Cell 2015, 161 (5), 988–97. [PubMed: 26000479]
3. Flemming HC; Wingender J, The biofilm matrix. Nat Rev Microbiol 2010, 8 (9), 62333.
4. Flemming HC; Wingender J; Szewzyk U; Steinberg P; Rice SA; Kjelleberg S, Biofilms: an emergent form of bacterial life. Nat Rev Microbiol 2016, 14 (9), 563–75. [PubMed: 27510863]
5. Stoodley P; Lewandowski Z; Boyle JD; Lappin-Scott HM, The formation of migratory ripples in a mixed species bacterial biofilm growing in turbulent flow. Environ Microbiol 1999, 1 (5), 447–55. [PubMed: 11207765]
6. Stoodley P; Lewandowski Z; Boyle JD; Lappin-Scott HM, Structural deformation of bacterial biofilms caused by short-term fluctuations in fluid shear: an in situ investigation of biofilm rheology. Biotechnol Bioeng 1999, 65 (1), 83–92. [PubMed: 10440674]
7. Rowlett VW; Mallampalli V; Karlstaedt A; Dowhan W; Taegtmeyer H; Margolin W; Vitrac H, Impact of Membrane Phospholipid Alterations in Escherichia coli on Cellular Function and Bacterial Stress Adaptation. J Bacteriol 2017, 199 (13).
8. Alsharif G; Ahmad S; Islam MS; Shah R; Busby SJ; Krachler AM, Host attachment and fluid shear are integrated into a mechanical signal regulating virulence in Escherichia coli O157:H7. Proc Natl Acad Sci U S A 2015, 112 (17), 5503–8. [PubMed: 25870295]
9. Kline KA; Falker S; Dahlberg S; Normark S; Henriques-Normark B, Bacterial adhesins in host-microbe interactions. Cell Host Microbe 2009, 5 (6), 580–92. [PubMed: 19527885]
10. Shi W; Sun H, Type IV pilus-dependent motility and its possible role in bacterial pathogenesis. Infect Immun 2002, 70 (1), 1–4. [PubMed: 11748156]
11. Silhavy TJ; Kahne D; Walker S, The bacterial cell envelope. Cold Spring Harb Perspect Biol 2010, 2 (5), a000414. [PubMed: 20452953]
12. Whitfield C; Trent MS, Biosynthesis and export of bacterial lipopolysaccharides. Annu Rev Biochem 2014, 83, 99–128. [PubMed: 24580642]

13. Nikaido H, Molecular basis of bacterial outer membrane permeability revisited. Microbiol Mol Biol Rev 2003, 67 (4), 593–656. [PubMed: 14665678]
14. Guidotti G, Membrane proteins. Annu Rev Biochem 1972, 41, 731–52. [PubMed: 4263713]
15. Jaroslawski S; Duquesne K; Sturgis JN; Scheuring S, High-resolution architecture of the outer membrane of the Gram-negative bacteria Roseobacter denitrificans. Mol Microbiol 2009, 74 (5), 1211–22. [PubMed: 19843216]
16. Singer SJ; Nicolson GL, The fluid mosaic model of the structure of cell membranes. Science 1972, 175 (4023), 720–31. [PubMed: 4333397]
17. Venable RM; Brown FL; Pastor RW, Mechanical properties of lipid bilayers from molecular dynamics simulation. Chem Phys Lipids 2015, 192, 60–74. [PubMed: 26238099]
18. Keten S; Xu Z; Ihle B; Buehler MJ, Nanoconfinement controls stiffness, strength and mechanical toughness of beta-sheet crystals in silk. Nat Mater 2010, 9 (4), 359–67. [PubMed: 20228820]
19. Krasnov I; Diddens I; Hauptmann N; Helms G; Ogurreck M; Seydel T; Funari SS; Muller M, Mechanical properties of silk: interplay of deformation on macroscopic and molecular length scales. Phys Rev Lett 2008, 100 (4), 048104. [PubMed: 18352338]
20. Tuszynski JA; Luchko T; Portet S; Dixon JM, Anisotropic elastic properties of microtubules. Eur Phys J E Soft Matter 2005, 17 (1), 29–35. [PubMed: 15864724]
21. Wells DB; Aksimentiev A, Mechanical properties of a complete microtubule revealed through molecular dynamics simulation. Biophys J 2010, 99 (2), 629–37. [PubMed: 20643083]
22. Zeiger AS; Layton BE, Molecular modeling of the axial and circumferential elastic moduli of tubulin. Biophys J 2008, 95 (8), 3606–18. [PubMed: 18621829]
23. Jo S; Kim T; Im W, Automated builder and database of protein/membrane complexes for molecular dynamics simulations. PLoS One 2007, 2 (9), e880. [PubMed: 17849009]
24. Jo S; Kim T; Iyer VG; Im W, CHARMM-GUI: a web-based graphical user interface for CHARMM. J Comput Chem 2008, 29 (11), 1859–65. [PubMed: 18351591]
25. Horst R; Stanczak P; Wuthrich K, NMR polypeptide backbone conformation of the E. coli outer membrane protein W. Structure 2014, 22 (8), 1204–9. [PubMed: 25017731]
26. Pautsch A; Schulz GE, High-resolution structure of the OmpA membrane domain. J Mol Biol 2000, 298 (2), 273–82. [PubMed: 10764596]
27. Prince SM; Achtman M; Derrick JP, Crystal structure of the OpcA integral membrane adhesin from Neisseria meningitidis. Proc Natl Acad Sci U S A 2002, 99 (6), 3417–21. [PubMed: 11891340]
28. Snijder HJ; Ubarretxena-Belandia I; Blaauw M; Kalk KH; Verheij HM; Egmond MR; Dekker N; Dijkstra BW, Structural evidence for dimerization-regulated activation of an integral membrane phospholipase. Nature 1999, 401 (6754), 717–21. [PubMed: 10537112]
29. Kucerka N; Liu Y; Chu N; Petrache HI; Tristram-Nagle S; Nagle JF, Structure of fully hydrated fluid phase DMPC and DLPC lipid bilayers using X-ray scattering from oriented multilamellar arrays and from unilamellar vesicles. Biophys J 2005, 88 (4), 2626–37. [PubMed: 15665131]
30. Wu EL; Fleming PJ; Yeom MS; Widmalm G; Klauda JB; Fleming KG; Im WE coli outer membrane and interactions with OmpLA. Biophys J 2014, 106 (11), 2493–502. [PubMed: 24896129]
31. Klauda JB; Venable RM; Freites JA; O'Connor JW; Tobias DJ; MondragonRamirez C; Vorobyov I; MacKerell AD, Jr.; Pastor RW, Update of the CHARMM allatom additive force field for lipids: validation on six lipid types. J Phys Chem B 2010, 114 (23), 7830–43. [PubMed: 20496934]
32. Phillips JC; Braun R; Wang W; Gumbart J; Tajkhorshid E; Villa E; Chipot C; Skeel RD; Kale L; Schulten K, Scalable molecular dynamics with NAMD. J Comput Chem 2005, 26 (16), 1781–802. [PubMed: 16222654]
33. York DM; Darden TA; Pedersen LG, The effect of long-range electrostatic interactions in simulations of macromolecular crystals: A comparison of the Ewald and truncated list methods. The Journal of Chemical Physics 1993, 99 (10), 8345–8348.
34. Lomize AL; Pogozheva ID; Lomize MA; Mosberg HI, Positioning of proteins in membranes: a computational approach. Protein Sci 2006, 15 (6), 1318–33. [PubMed: 16731967]

35. Lomize MA; Lomize AL; Pogozheva ID; Mosberg HI, OPM: orientations of proteins in membranes database. Bioinformatics 2006, 22 (5), 623–5. [PubMed: 16397007]
36. Landau LD; Lifschit EM, Theory of elasticity, vol 7 New York, 1970.
37. Marx DC; Fleming KG, Influence of Protein Scaffold on Side-Chain Transfer Free Energies. Biophys J 2017, 113 (3), 597–604. [PubMed: 28793214]
38. Moon CP; Fleming KG, Side-chain hydrophobicity scale derived from transmembrane protein folding into lipid bilayers. Proc Natl Acad Sci U S A 2011, 108 (25), 10174–7. [PubMed: 21606332]
39. Moon CP; Zaccai NR; Fleming PJ; Gessmann D; Fleming KG, Membrane protein thermodynamic stability may serve as the energy sink for sorting in the periplasm. Proc Natl Acad Sci U S A 2013, 110 (11), 4285–90. [PubMed: 23440211]
40. Miyashita O; Onuchic JN; Wolynes PG, Nonlinear elasticity, proteinquakes, and the energy landscapes of functional transitions in proteins. Proc Natl Acad Sci U S A 2003, 100 (22), 12570–5. [PubMed: 14566052]
41. Kol N; Adler-Abramovich L; Barlam D; Shneck RZ; Gazit E; Rousso I, Self-assembled peptide nanotubes are uniquely rigid bioinspired supramolecular structures. Nano Lett 2005, 5 (7), 1343–6. [PubMed: 16178235]
42. Niu L; Chen X; Allen S; Tendler SJ, Using the bending beam model to estimate the elasticity of diphenylalanine nanotubes. Langmuir 2007, 23 (14), 7443–6. [PubMed: 17550276]
43. Picas L; Rico F; Scheuring S, Direct measurement of the mechanical properties of lipid phases in supported bilayers. Biophys J 2012, 102 (1), L01–3. [PubMed: 22225813]
44. Ivanovska IL; de Pablo PJ; Ibarra B; Sgalari G; MacKintosh FC; Carrascosa JL; Schmidt CF; Wuite GJ, Bacteriophage capsids: tough nanoshells with complex elastic properties. Proc Natl Acad Sci U S A 2004, 101 (20), 7600–5. [PubMed: 15133147]
45. Greaves GN; Greer AL; Lakes RS; Rouxel T, Poisson's ratio and modern materials. Nat Mater 2011, 10 (11), 823–37. [PubMed: 22020006]
46. Rawicz W; Olbrich KC; McIntosh T; Needham D; Evans E, Effect of chain length and unsaturation on elasticity of lipid bilayers. Biophys J 2000, 79 (1), 328–39. [PubMed: 10866959]
47. Rassam P; Copeland NA; Birkholz O; Toth C; Chavent M; Duncan AL; Cross SJ; Housden NG; Kaminska R; Seger U; Quinn DM; Garrod TJ; Sansom MS; Piehler J; Baumann CG; Kleanthous C, Supramolecular assemblies underpin turnover of outer membrane proteins in bacteria. Nature 2015, 523 (7560), 333–6. [PubMed: 26061769]
48. Koebnik R; Locher KP; Van Gelder P, Structure and function of bacterial outer membrane proteins: barrels in a nutshell. Mol Microbiol 2000, 37 (2), 239–53. [PubMed: 10931321]
49. Wiśniewski JR; Rakus D, Multi-enzyme digestion FASP and the 'Total Protein Approach'-based absolute quantification of the Escherichia coli proteome. Journal of Proteomics 2014, 109, 322–331. [PubMed: 25063446]
50. Wang Y, The Function of OmpA in Escherichia coli. Biochemical and Biophysical Research Communications 2002, 292 (2), 396–401. [PubMed: 11906175]
51. Dekker N; Tommassen J; Lustig A; Rosenbusch JP; Verheij HM, Dimerization regulates the enzymatic activity of Escherichia coli outer membrane phospholipase A. J Biol Chem 1997, 272 (6), 3179–84. [PubMed: 9013551]
52. Gil F; Ipinza F; Fuentes J; Fumeron R; Villarreal JM; Aspée A; Mora GC; Vásquez CC; Saavedra C, The ompW (porin) gene mediates methyl viologen (paraquat) efflux in Salmonella enterica serovar Typhimurium. Research in Microbiology 2007, 158 (6), 529–536. [PubMed: 17618087]
53. Hong H; Patel DR; Tamm LK; van den Berg B, The outer membrane protein OmpW forms an eight-stranded beta-barrel with a hydrophobic channel. J Biol Chem 2006, 281 (11), 7568–77. [PubMed: 16414958]
54. Wu X-B; Tian L-H; Zou H-J; Wang C-Y; Yu Z-Q; Tang C-H; Zhao F-K; Pan J-Y, Outer membrane protein OmpW of Escherichia coli is required for resistance to phagocytosis. Research in Microbiology 2013, 164 (8), 848–855. [PubMed: 23811183]
55. Boulbitch A; Quinn B; Pink D, Elasticity of the rod-shaped gram-negative eubacteria. Phys Rev Lett 2000, 85 (24), 5246–9. [PubMed: 11102232]

56. Vollmer W; Holtje JV, The architecture of the murein (peptidoglycan) in gramnegative bacteria: vertical scaffold or horizontal layer(s)? J Bacteriol 2004, 186 (18), 5978–87. [PubMed: 15342566]

57. Vollmer W; Blanot D; de Pedro MA, Peptidoglycan structure and architecture. FEMS Microbiol Rev 2008, 32 (2), 149–67. [PubMed: 18194336]

58. Thwaites JJ; Mendelson NH, Mechanical properties of peptidoglycan as determined from bacterial thread. Int J Biol Macromol 1989, 11 (4), 201–6. [PubMed: 2518734]

59. Thwaites JJ; Mendelson NH, Biomechanics of bacterial walls: studies of bacterial thread made from Bacillus subtilis. Proc Natl Acad Sci U S A 1985, 82 (7), 2163–7. [PubMed: 3920662]

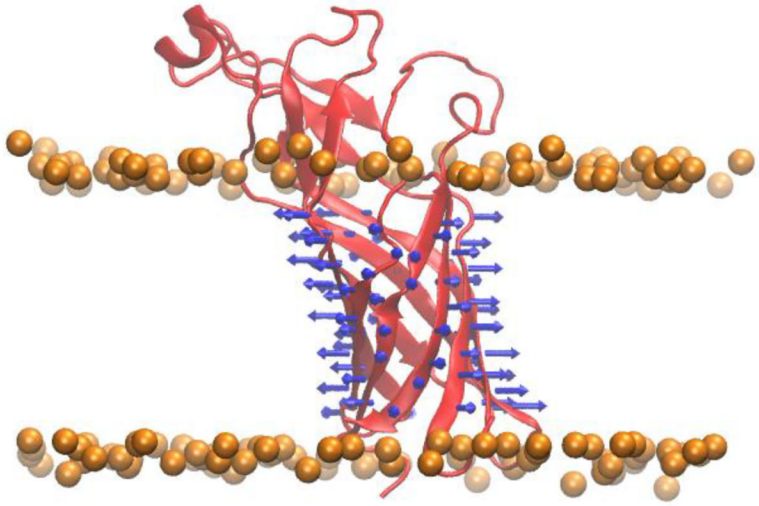

Figure 1.

User defined mechanical forces were applied to deform the transmembrane β-barrel. Representation of force vectors (dark blue) on the OmpW structure (red) as they are applied during the simulation. The plane of the membrane is designated with spheres representing the phosphate atoms (orange) of the DMPC molecules. The figure was created using VMD.

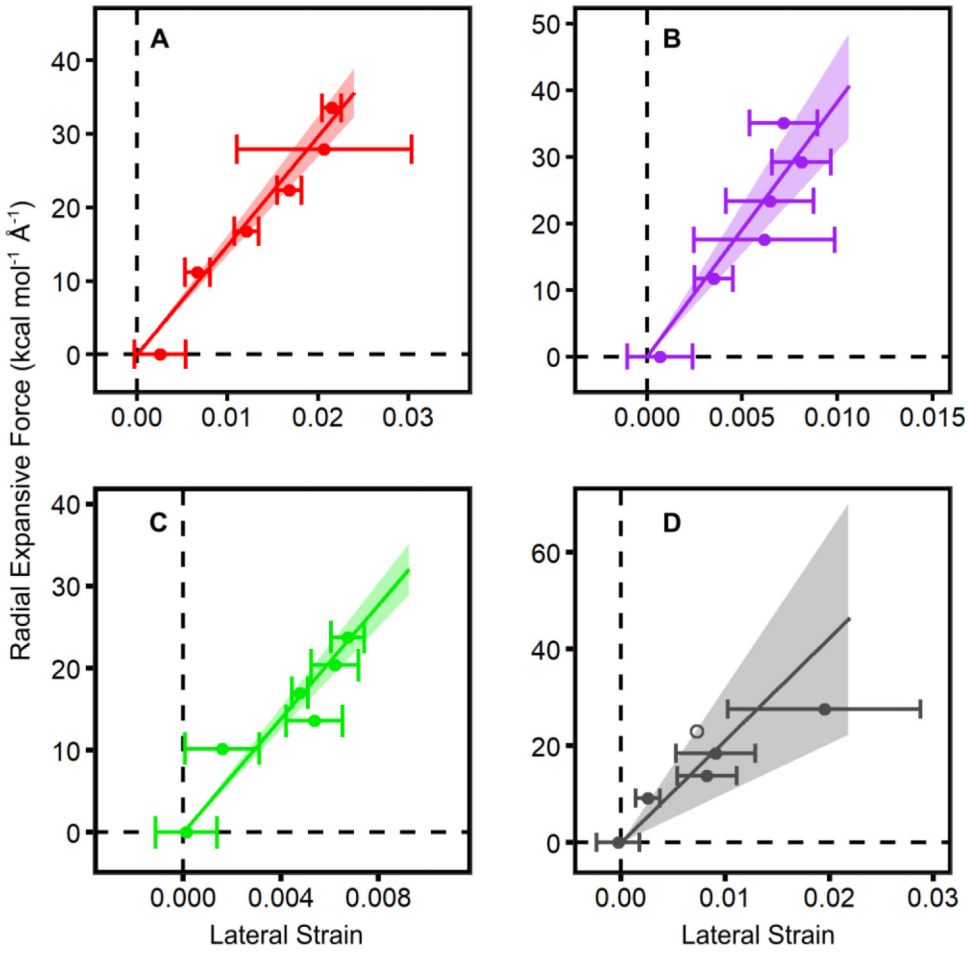

Figure 2.

All OMPs demonstrate a linear response to applied radial expansive stress (R^2 = 0.99 (*A, OmpW*), 0.97 (*B, OmpA*), 0.99 (*C, OpcA*), 0.88 (*D, OmpLA*)). Points represent average lateral strain from two to three independent simulations. Error bars represent the standard error of the mean. Solid line represents the best fit line and the shaded region denotes 95% confidence bands of the linear fit. The unfilled points represent the average barrel strain from only one simulation and are omitted from the fit because of undetermined error.

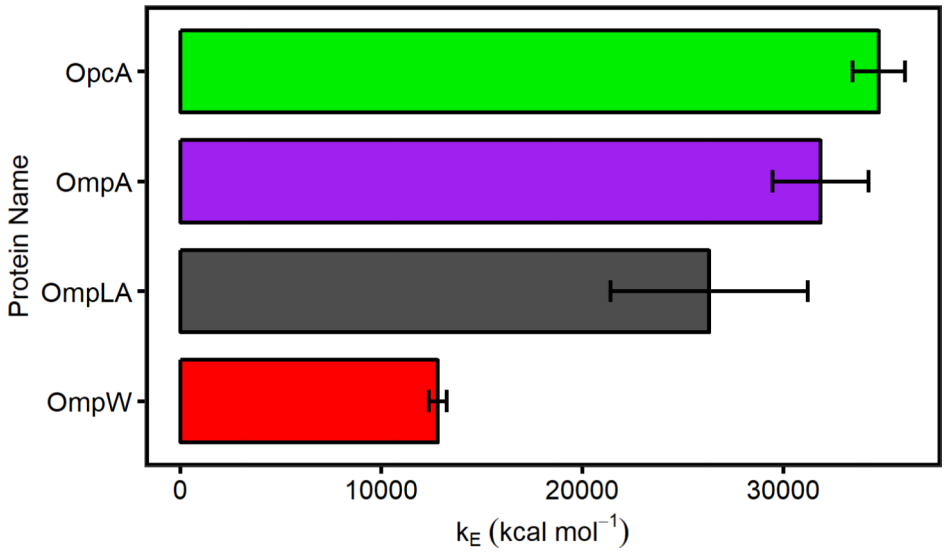

Figure 3:

OMPs are energetically rigid. The values of the elasticity constant k_E are large (OmpW (12800 ± 460 kcal mol^{-1}), OmpA (32000 ± 2400 kcal mol^{-1}), OpcA (35000 ± 1300 kcal mol^{-1}), and OmpLA (26000 ± 4900 kcal mol^{-1})). Error bars are 95% confidence intervals from the linear fit.

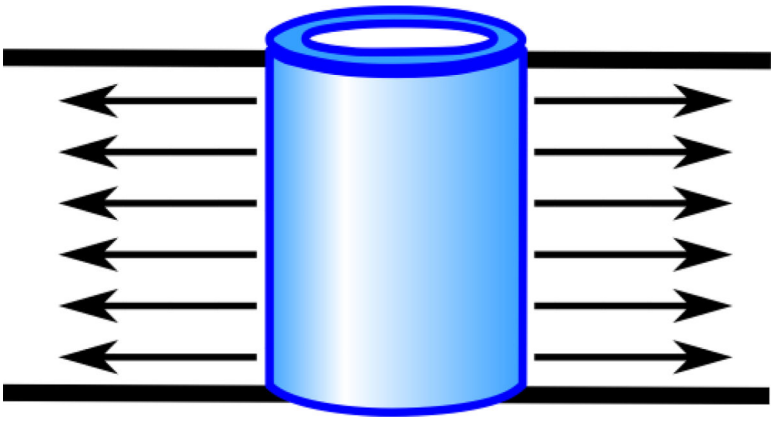

Figure 4.

A hollow cylindrical shell representing the geometric model used for calculating OMP elasticity by approximating the backbone volume. The thick black lines are meant to represent the boundary of the plane of the phosphates and denote the transmembrane region of the protein. The thin black arrows represent the direction of the applied expansive force.

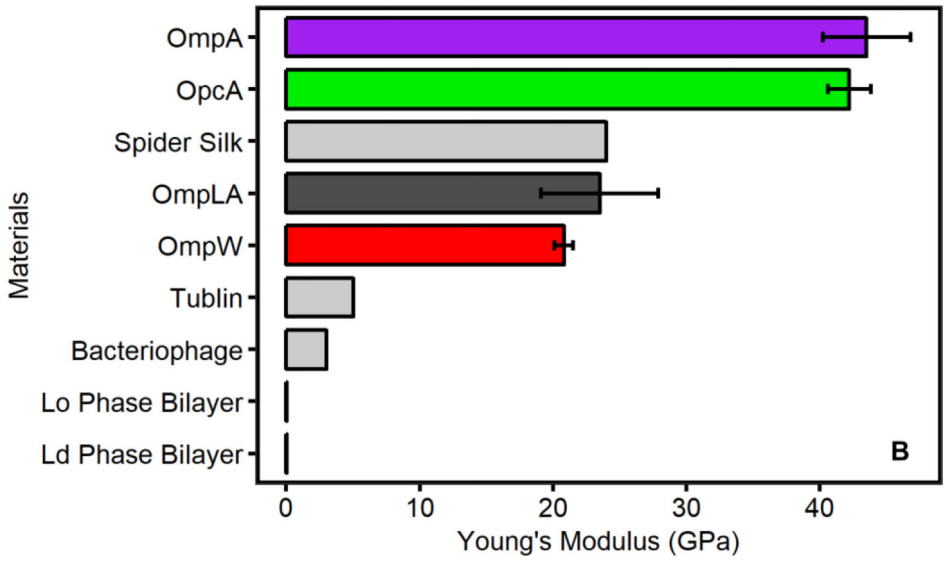

Figure 5.

OMPs display very rigid elastic parameters. The Young's moduli (*E*) of OMPs are similar in magnitude to other β-sheet proteins such as spider silk and more than three orders of magnitude larger than phospholipid bilayers.[18–22, 43–44]

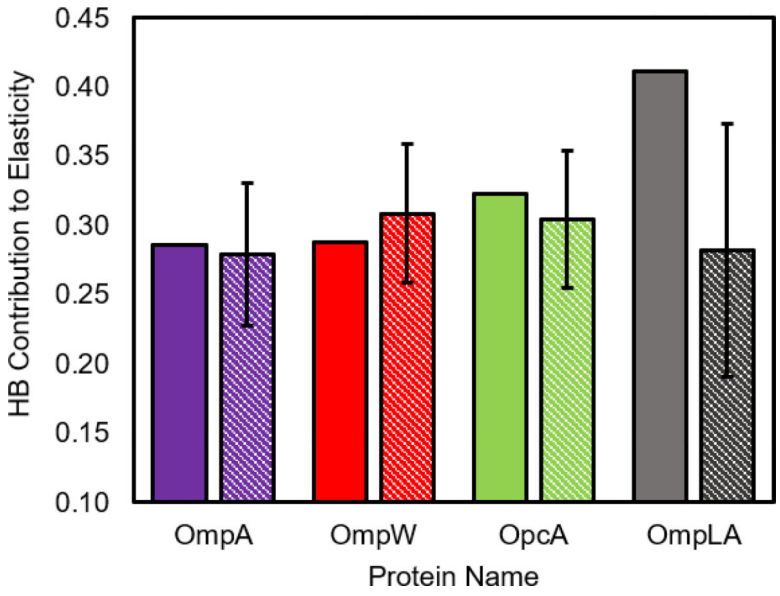

Figure 6:

Backbone HBs account ~30% of OMP elasticity. The contribution of backbone HBs to the value of k_E was calculated by multiplying the value of $k_{E,HB}$ by the number of transmembrane HBs and then dividing it by the value of k_E. Solid bars represent the contribution using the value of $k_{E,HB}$ calculated from HB fluctuations, and patterned bars represent the contribution of backbone HBs using the value of $k_{E,HB}$ calculated from linear regression of HB stress vs strain graph (see Supplemental Information). Error bars represent the 95% confidence interval from the linear regression. With the exception of the OmpLA fluctuations contribution, all values are within error of one another and make up approximately ~30%.

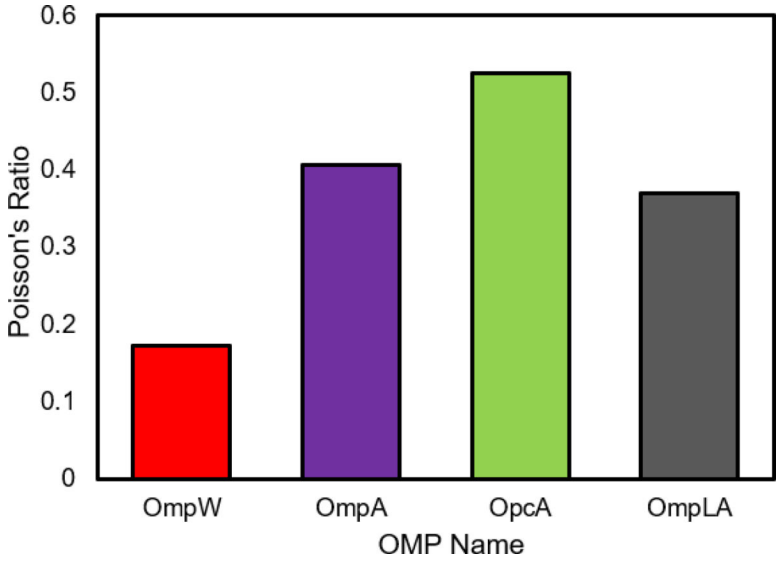

Figure 7:

Poisson's ratio of OMPs are positive and indicate that expansive forces in the membrane cause the protein to decrease in height. The values for the Poisson's value are (0.172 (OmpW), 0.407 (OmpA), 0.526 (OpcA), 0.406(OmpLA)).

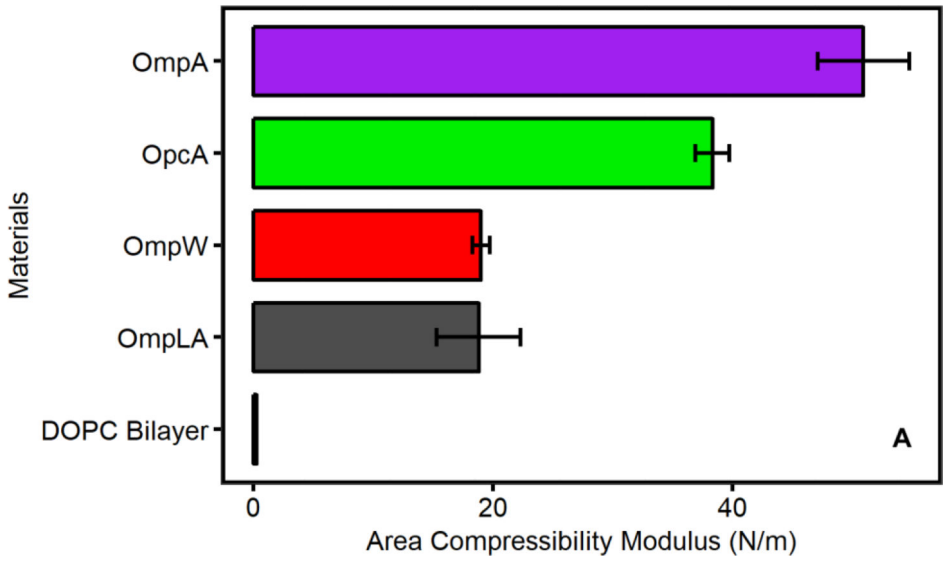

Figure 8:
OMPs will rigidify bilayers. The value of the area compressibility moduli of OMPs is between 70 and 190 times greater than that of a lipid bilayer patch.[46]